Calculation of low-energy-electron-diffraction intensities from ZnO ($10\bar{1}0$). II. Influence of calculational procedure, model potential, and second-layer structural distortions

C. B. Duke, R. J. Meyer, and A. Paton
Xerox Webster Research Center, Xerox Square-W114, Rochester, New York 14644

P. Mark
Department of Electrical Engineering, Princeton University, Princeton, New Jersey 08540
(Received 24 March 1978)

Dynamical calculations of the intensities of normally-incident low-energy electrons diffracted from ZnO($10\bar{1}0$), performed using an "exact" matrix-inversion method, are compared both with earlier calculations based on the renormalized-forward-scattering (RFS) method and with measured intensities. The sensitivity of the calculated intensities to the choice of model potential and the magnitude of thermal atomic vibrations is displayed within the context of examining the implications of uncertainties in nonstructural model parameters on surface-structure determinations via elastic low-energy-electron diffraction (ELEED) intensity analyses. We extend our earlier analysis of the surface structure of ZnO($10\bar{1}0$) by utilizing the matrix inversion rather than RFS method, a recently revised bulk geometry for ZnO, an improved model potential, and a consideration of second-as well as top-layer structural distortions. The combination of these four improvements lead to the selection of the most probable surface structure for ZnO($10\bar{1}0$) as one in which the top-layer oxygen is displaced vertically downward by $\Delta d_{\perp}(\mathrm{O}) = -0.05 \pm 0.1$ Å and the top-layer zinc likewise by $\Delta d_{\perp}(\mathrm{Zn}) = -0.45 \pm 0.1$ Å. No compelling evidence either for lateral distortions within the top layer or for second-layer distortions is obtained, although small improvements in the agreement between the calculated and observed intensities can be achieved by considering them. Our major conclusion is that given the limitations in the available ELEED intensity data and the uncertainties in the model potential and surface atomic vibrations, the vertical distortion cited above constitute the maximum structural information that can be extracted unambiguously via ELEED intensity analysis at the present time.

I. INTRODUCTION

In a series of earlier papers[1-4] we described the use of elastic low-energy-electron-diffraction (ELEED) intensity analysis to determine the atomic geometry of the low-index faces of ZnO and the unique position of ZnO at the boundary between "ionic" and "covalent" semiconductors as determined from their bulk structure (i.e., cubic versus tetrahedrally coordinated). Since the performance of these early calculations, however, a number of computational and conceptual issues have arisen during the course of ELEED studies of other semiconductor surfaces,[5,6] and a new structure of bulk ZnO (see Ref. 7) has been called to our attention.[8] Our purpose in this paper is the presentation of a new and considerably expanded ELEED intensity analysis for ZnO($10\bar{1}0$), the truncated bulk structure of which is shown in Fig. 1. In particular, we utilize a set of computer programs based on the matrix inversion multiple-scattering method,[1,9] which both avoids the need for the approximate renormalized-forward-scattering (RFS) method used earlier,[2] and permits the examination of reconstructions from the bulk geometry of the second (and deeper) atomic layers as well as the uppermost layer. We also consider the issue, raised by recent analyses of ELEED from MgO (Ref. 10) and NiO,[11] of the nature and magnitude

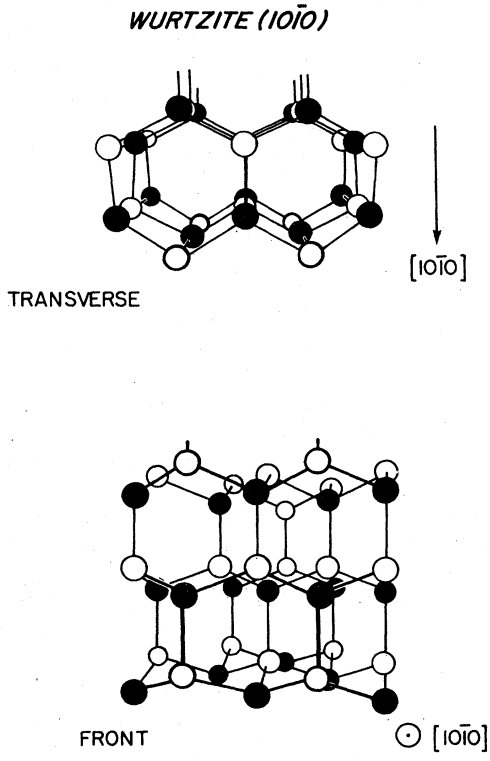

FIG. 1. Schematic diagram of the side (upper panel) and front (lower panel) view of an unreconstructed surface of ZnO($10\bar{1}0$).

of uncertainties in semiconductor structure determinations via ELEED intensity analyses caused by corresponding uncertainties in the model potential. Finally, the analysis reported herein embodies both the most recent bulk structure of ZnO,[7] rather than that given by Wyckoff,[12] and a revised value for the Debye temperature $\Theta_D = 385°K$, which is the average of several measured values[7,13,14] of this quantity.

We proceed in three steps. Our model calculations and their sensitivity to the values of the nonstructural parameters are described in Sec. II. Section III is devoted to the presentation of the results of our structure analysis of ZnO($10\bar{1}0$). Initially only top-layer reconstructions are considered. Then, the extension of this analysis to incorporate second-layer reconstructions is given. We conclude with a synopsis of our results.

II. MODEL CALCULATIONS: SENSITIVITY ANALYSIS

This section is devoted to descriptions of the model electron-solid interaction, the computational procedure utilized to evaluate the ELEED intensities, and the influence on the predicted intensities of the computational procedure and of the values of the nonstructural parameters. Each of these topics is considered below.

A. Electron-solid interaction

The model electron-solid interaction is specified in terms of three types of parameters: those describing the electron–ion-core potential in a rigid lattice, those describing the electron-electron-interaction-induced "optical" potential, and those describing the thermal motions of the ion cores. We discuss each in turn.

The electron–ion-core interaction in a rigid lattice is described by a one-electron muffin-tin potential. Specifically, we consider a model consisting of spherically symmetrical ion-core potentials within individual layers of the solid parallel to its surface.[9,15-17] For such potentials the scattering of the electrons from an individual ion core is specified by a sequence of phase shifts $\{\delta_l(E)\}$, which depend on the angular momentum $L = l\hbar$ and energy E of the incident electron relative to the scatterer. All electron–ion-core interaction potentials are characterized by calculating the phase shifts (for $l \leq 10$ and energies in the range $0 < E < 180$ eV) by numerical integration of the Schrödinger equations associated with the individual ion cores. In our dynamical calculations of the ELEED intensities, however, only the first four phase shifts, $l \leq 3$, were used, a restriction whose validity was verified explicitly by Duke *et al.*[4]

The ion-core potentials are evaluated using an overlapping atomic charge density model.[18] This task is accomplished in two steps. First, the crystal potential $V_c(r)$ is calculated, and then it is reduced to the muffin-tin form for evaluation of the phase shifts. A local (Slater-exchange) approximation[19] is used for the exchange terms in the potential. To evaluate the crystal potential we utilized the charge densities associated with singly ionic species, i.e., Zn^+O^-. For fixed muffin-tin radii, the ionic or atomic nature of the charge densities exert rather little influence on the resulting phase shifts and ELEED intensities.[4] The crystal potentials are different for the Wyckoff[12] and Abrahams-Bernstein[7] ZnO crystal structures, however, both because of the different atomic distances involved in the computation of the crystal charge density,[18] and because the Madelung constants depend implicitly on the structural parameters.[20] Numerical evaluation of the Madelung constants revealed that the latter effect was only a few percent, however, so we utilized the value for an ideal tetrahedrally coordinated zinc-blende lattice[20] in evaluating the crystal potential. Cross-sectional views of the crystal potentials taken through a Zn–O bond in a plane parallel to the ($10\bar{1}0$) surface (see, e.g., Fig. 1) are shown in Fig. 2. Model 1 refers to the Abrahams-Bernstein structure[7] [nearest-neighbor $d(\text{ZnO}) = 1.973$ Å] and model 2 to the Wyckoff structure[12] [$d(\text{Zn–O}) = 1.8$ Å]. Duke *et al.* utilized the atomic radii[21] $d_A(\text{O}) = 0.6$ Å and $d_A(\text{Zn}) = 1.35$ Å as the muffin-tin radii for the Wyckoff structure. While this choice is acceptable for atomic potentials, it is evident from Fig. 2 that it greatly underestimates the O^- potential and overestimates the Zn^+ potential. Therefore, as described in our analyses for[22] GaAs and ZnSe,[23] we select the crossover point in the crystal potential along the nearest-neighbor bond as determining both the muffin-tin radii and constant potential outside the muffin-tin spheres. This procedure leads to the values $r_{\text{MT}}(\text{O}) = 0.91$ Å and $r_{\text{MT}}(\text{Zn}) = 1.063$ Å for Abrahams-Bernstein structure. These values of the muffin-tin radii and the crystal potential shown in Fig. 2 yield the phase shifts labeled by model 1 in Figs. 3 and 4 for the Zn^+ and O^- species, respectively. The phase shifts resulting from the crystal potential obtained for the Wyckoff structure and the Slater atomic radii are labeled as model 2 in these figures. Although a Korringa-Kohn-Rostoker (KKR) band-structure calculation has been reported[24] for ZnO, neither the potential nor the phase shifts were given in that paper so that a direct comparison with ours is impossible.

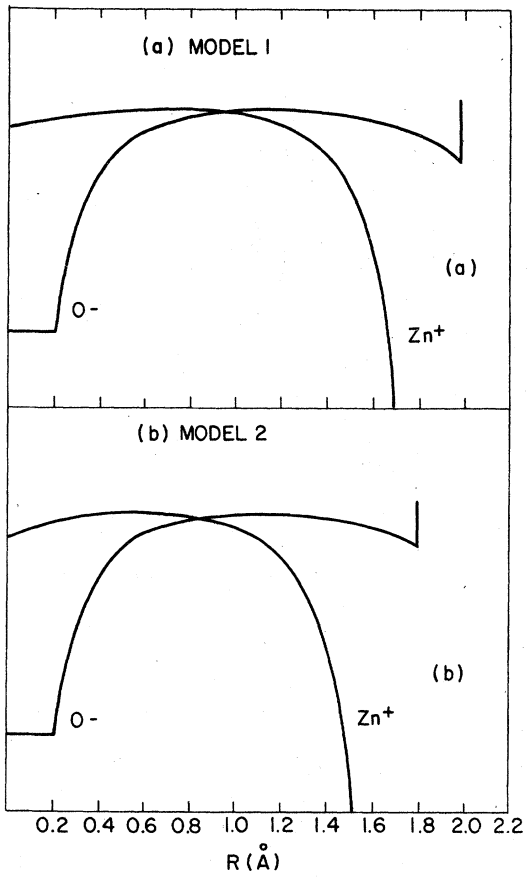

FIG. 2. Model crystal potentials utilized to calculate the phase shifts used in the low-energy-electron-diffraction structure analysis of ZnO($10\bar{1}0$). Panel (a): the model potential (model 1) used herein based on the bulk crystal structure of Abrahams and Bernstein (Ref. 7). Potential crossover radii are $r(\mathrm{Zn}) = 1.063$ Å and $r(0) = 0.9$ Å corresponding to a Zn–O nearest-neighbor distance of 1.973 Å. Panel (b): the model potential (model 2) used by Duke *et al.* (Ref. 4) based on the bulk crystal structure given by Wyckoff (Ref. 12). The Zn^+ and O^- potentials are equal at a distance corresponding to $r(\mathrm{Zn}) = 0.96$ Å and $r(\mathrm{O}) = 0.84$ Å. The Zn–O nearest-neighbor distance in this structure is $r(\mathrm{Zn}) + r(\mathrm{O}) = 1.8$ Å.

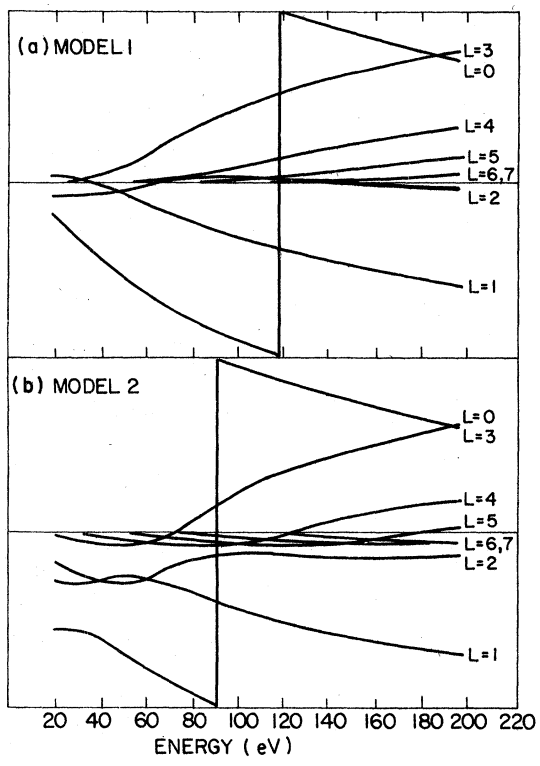

FIG. 3. Phase shifts for the Zn^+ species obtained using the muffin-tin radii of 1.063 Å [panel (a), phase shifts used herein] and 1.35 Å [panel (b), phase shifts used by Duke *et al.* (Ref. 4)].

The zero-force criterion[25] used to obtain the muffin-tin radii in that calculation produces, however, identical radii to the potential-crossing criterion utilized in model 1. The qualitative features of the KKR energy-band structure are in satisfactory agreement with reflectivity[26] and photoemission[27] data. Quantitatively, the valence-band structure is too narrow and the d states lie too high in energy.

The optical potential associated with the electron-electron interactions is taken to be spatially uniform outside the muffin-tin spheres and to assume the form

$$\Sigma(E) = -V_0 - i\hbar[2m(E+V_0)]^{1/2}/m\lambda_{ee}\,, \tag{1}$$

in which V_0 is the real "inner potential" and λ_{ee} is the inelastic-collision damping length.[28] We select $V_0 = 10$ eV and $\lambda_{ee} = 8$ Å as in our prior analyses.[1-4]

The final parameters which we must specify are those associated with the vibrational motion of the atomic scatterers. This motion is incorporated into the calculation of the ELEED intensities by a renormalization of the rigid-lattice electron–ion-core vertex. In the case of a rigid lattice these vertices are given by[9]

$$t_\nu(\vec{k}', \vec{k}) = \frac{4\pi^2 i\hbar^2}{mk(E)} \sum_{l,m} \{\exp[2i\delta_l^\nu(E)] - 1\} \times Y_{lm}^*(\hat{k}')Y_{lm}(\hat{k})\,, \tag{2a}$$

$$k^2(E) = 2m[E - \Sigma(E)]/\hbar^2\,. \tag{2b}$$

The index ν labels the layer parallel to the surface in which the ion core is found and $\hat{k}$ is a unit vector in the direction of $\vec{k}$. The $\delta_l^\nu(E)$ may depend explicitly on this index. The consequences of the atomic vibrations of the lattice are introduced, in

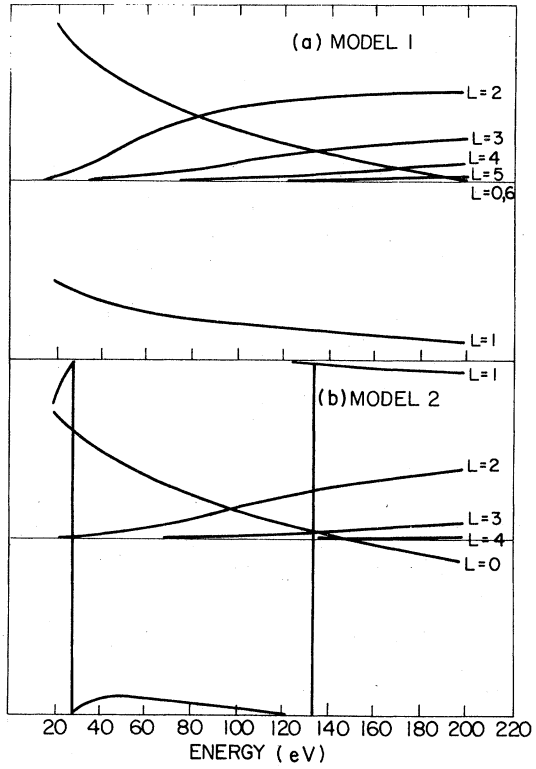

FIG. 4. Phase shifts for the O^- species obtained using the muffin-tin radii of 0.91 Å [panel (a), phase shifts used herein] and 0.60 Å [panel (b), phase shifts used by Duke *et al.* (Ref. 4)].

an approximate way,[16] by the multiplication of the rigid-lattice t vertices by the associated Debye-Waller factors. Using the spherical Debye model of the lattice-vibration spectra, we get

$$b_\nu(\vec{k}', \vec{k}) = t_\nu(\vec{k}', \vec{k}) \exp[-2(k' - k)^2 W_\nu(T)], \quad (3a)$$

$$W_\nu(T) = \frac{3\hbar^2}{2M_\nu \kappa \Theta_D^\nu} \left[\frac{1}{4} + \left(\frac{T}{\Theta_D^\nu} \right)^2 \int_0^{\Theta_D^\nu / T} \frac{x\,dx}{e^x - 1} \right], \quad (3b)$$

in which M_ν is the mass of the atoms in the layer labeled by ν, Θ_D^ν is the Debye temperature describing the motion of the atoms in this layer, T is the temperature, and κ is Boltzmann's constant. The quantity $b_\nu(\vec{k}', \vec{k})$ is the renormalized electron–ion-core vertex which is expanded into partial-wave components in multiple-scattering calculations of ELEED intensities. We use the value $\Theta_D = 385$°K for all layers. This is the average value of several measurements[13,14] of this quantity in bulk ZnO.

B. Computational procedure

The matrix-inversion (MI) computer programs used to perform the calculations of ELEED intensities from ZnO(10$\bar{1}$0) are extended versions of those described by Laramore and Duke.[9] The scattering from each translationally equivalent subplane is calculated in the angular momentum representation. The interference between subplanes is described by a matrix equation[9,15–17]

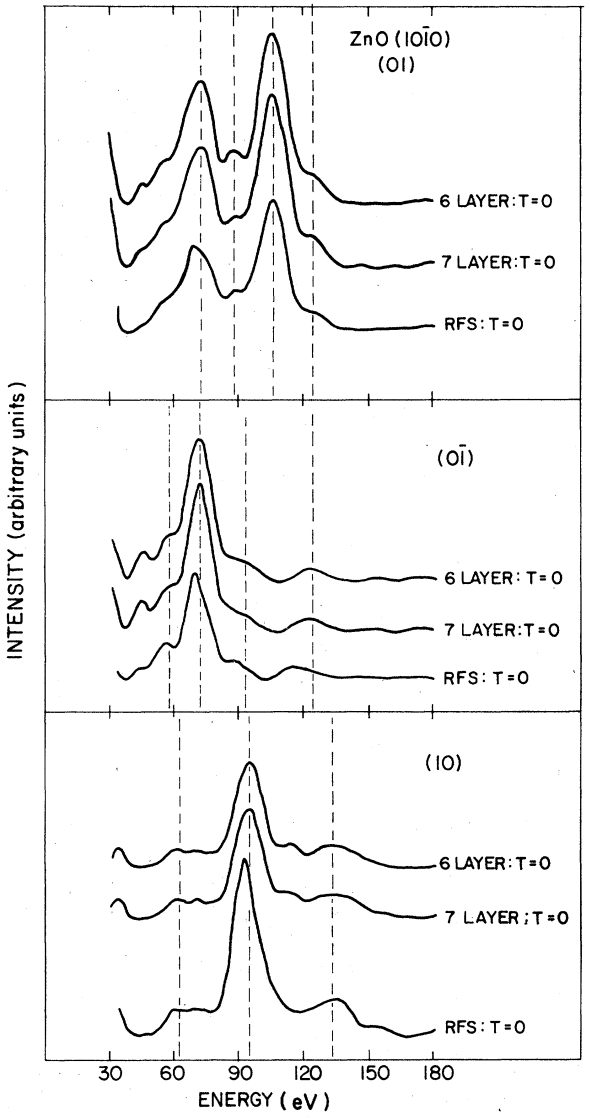

FIG. 5. Comparison of the predicted normal-incidence intensities obtained using the MI program and the RFS program used by Duke *et al.* (Ref. 4). The MI results are shown for both six and seven layers in order to display that the model predictions have converged at six layers. All Calculations are for normally incident electrons. The three panels contain the results for the three interior beams, (01), (0$\bar{1}$), and (10) = ($\bar{1}$0), respectively. The various calculational procedures are indicated beside the associated intensities in the figure. The phase shifts were obtained using model 2 described in the text.

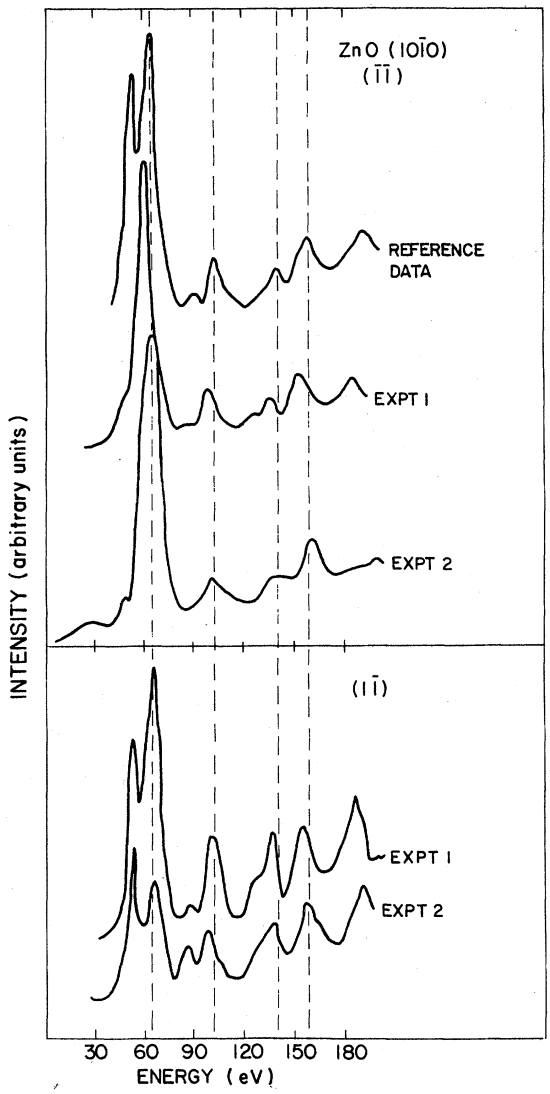

FIG. 6. Comparison of independent measurements of the intensities of the ($\bar{1}\bar{1}$) beam and its symmetry equivalent ($1\bar{1}$) beam for normally incident electrons diffracted from ZnO(10$\bar{1}$0) at room temperature. Since these data are those used in our earlier analyses, their acquisition is described in those works (Refs. 2–4, 29).

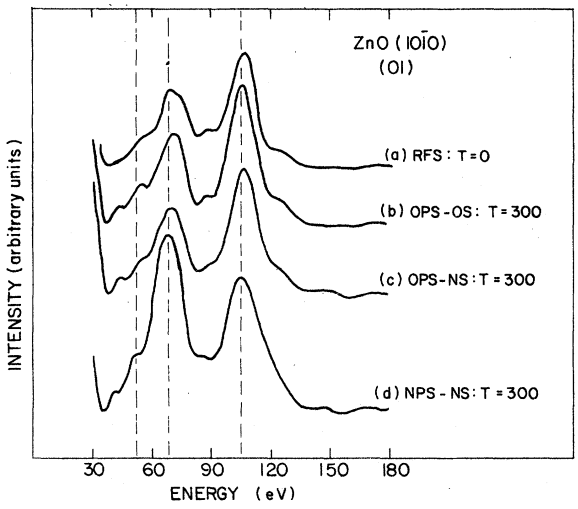

FIG. 7. Comparison of calculated intensities for the (01) beam of normally incident electrons diffracted from ZnO(10$\bar{1}$0) obtained using various computational procedures and input parameters. Curve (a): zero temperature, RFS method, OPS from Duke *et al.*, (Ref. 4) original (unreconstructed) surface structure (OS) from Wyckoff (Ref. 12). Curve (b): MI program, $T = 300\,^{\circ}\mathrm{K}$ but otherwise identical parameters to those used to obtain curve (a). Curve (c): same as curve (b) but using the new (unreconstructed) bulk structure (NS) given by Abrahams and Berstein (Ref. 7). Curve (d): same as curve (c) but using the NPS obtained from model 1, described in the text.

which is solved numerically for a model crystal consisting of a finite number of layers. Since the interference between the subplanes is accounted for by a MI technique, the positions of the subplanes are arbitrary so that distortions from the ideal bulk geometry may be accommodated (at no additional computational expense) to any depth within the sample. In the calculations reported herein we utilize four ($l \leq 3$) phase shifts to describe the O^- and Zn^+ scatterers within the individual subplanes. The results achieved thereby are nearly identical to those obtained with six phase shifts,[4] but cost less than one-quarter as much to run on the computer because the cost of operating the MI program scales as $(l_{\max}+1)^4$.

A comparison of the $T = 0$ limit of the MI calculations with our earlier[4] RFS rigid-lattice calculations is shown in Fig. 5 for an unreconstructed bulk geometry of ZnO(10$\bar{1}$0) and the phase shifts obtained using model 2. For some beams, e.g., the (01) beam, the two methods give essentially identical results. For others, e.g., the (10) beam, the results are not identical but the differences are insignificant from the perspective of surface-structure determination. This is the most usual situation. We find that for the (0$\bar{1}$) beam, however, the differences between the intensities predicted by the two methods are substantial (e.g., the peak near 120 eV is shifted by 10 eV in the RFS as opposed to the MI method). Moreover, these differences lie well outside any truncated effects caused by the finite sample thickness used in the MI method, as shown explicitly in Fig. 5 by virtue of the presentation of calculated intensities for model samples six and seven layers thick, respectively. It is evident from the figures that for $\lambda_{ee} = 8$ Å, the MI results are fully converged for a six-layer-thick sample, which is the model

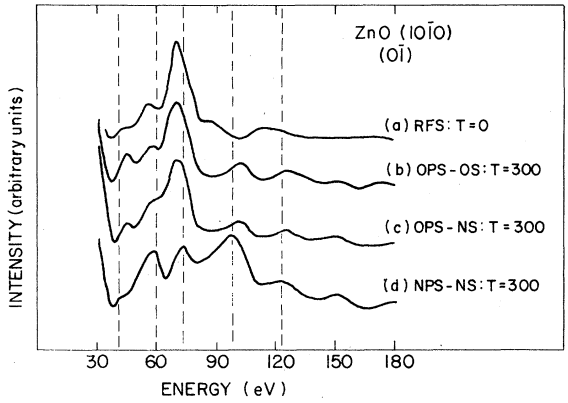

FIG. 8. Comparison of calculated intensities for the (0$\bar{1}$) beam of normally incident electrons diffracted from ZnO(10$\bar{1}$0) obtained using various computational procedures and input parameters. Curve (a): zero temperature, RFS method, OPS from Duke *et al.*, (Ref. 4) OS from Wyckoff (Ref. 12). Curve (b): MI program, $T = 300$ °K but otherwise identical parameters to those used to obtain curve (a). Curve (c): same as curve (b) but using the NS given by Abrahams and Bernstein (Ref. 7). Curve (d): same as curve (c) but using the NPS obtained from model 1, described in the text.

used in the remaining computations reported herein.

The geometry of the surface unit mesh used to index the beams shown in Fig. 5 and in the other figures in this paper is the same as that used by Duke *et al.*[4] It is described in Fig. 3 of their paper.[4]

C. Sensitivity analysis

In any surface-structure determination via ELEED intensity analysis, a number of features of the model calculations are selected which are not related directly to the surface atomic geometry. In our case these include the computational method (RFS versus MI), the choice of muffin-tin potential (model 1 versus model 2) and the inclusion of lattice vibrations (rigid lattice versus $T = 300$ K based on $\Theta_D = 385$ K), as well as the model for the optical potential. Moreover, for historial reasons we wish to assess the magnitudes of the consequences of these choices relative to those associated with the use of the Wyckoff[12] versus the Abrahams-Bernstein[7] geometries of bulk ZnO. This subsection is devoted to such an assessment.

The first important ingredient in this assessment, to which we refer as a sensitivity analysis,[5,6] is the establishment of the degree of reproducibility of the ELEED intensity data that is to be utilized in the surface-structure determination based on the model calculation. Independently

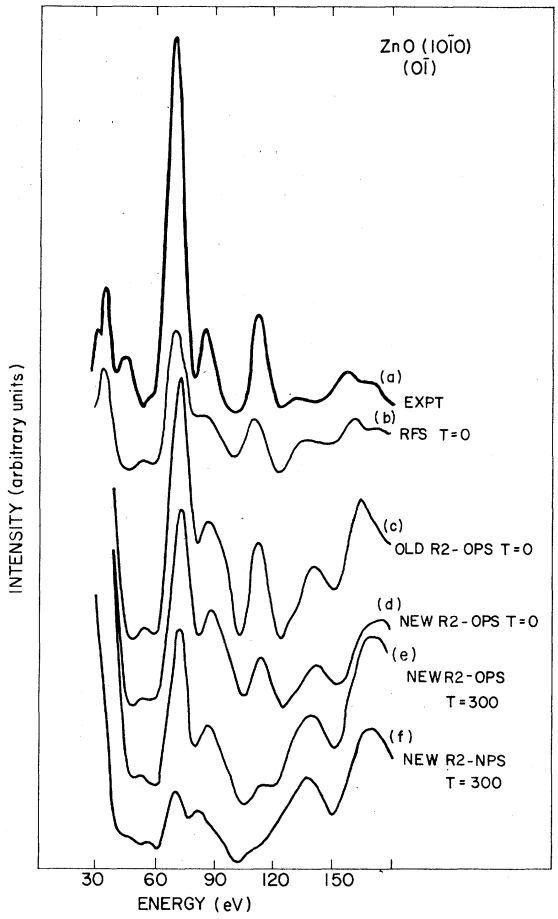

FIG. 9. Comparison of measured and calculated intensities of normally incident electrons diffracted into the (0$\bar{1}$) beam from ZnO(10$\bar{1}$0). Curve (a): measured intensities at $T = 300$ °K. Curve (b): RFS computation for a rigid lattice based on the OPS used by Duke *et al.* (Ref. 4) and the R2 reconstruction of the OS of Wyckoff (Ref. 12). Curve (c): the MI calculation utilizing the same model parameters as the RFS calculation shown in curve (b). Curve (d): rigid-lattice MI calculation based on the R2 reconstruction of the new (bulk) structure of Abrahams and Bernstein (Ref. 7). Curve (e): same as curve (d) but for $T = 300$ K. Curve (f): same as curve (e) but utilizing the NPS obtained from model 1, described in the text.

measured room-temperature intensities from separate samples for a typical nonspecular beam and its symmetry-equivalent beam are shown in Fig. 6. These data are those used in our earlier structure analyses of ZnO(10$\bar{1}$0), and their acquisition is described elsewhere.[2-4,29] While the results are self-explanatory, it is worth noting the serious reproducibility problems for incident electron energies below about 60 eV. These resulted from the instrumentation used at the time,[29] and could almost certainly be reduced by repeated

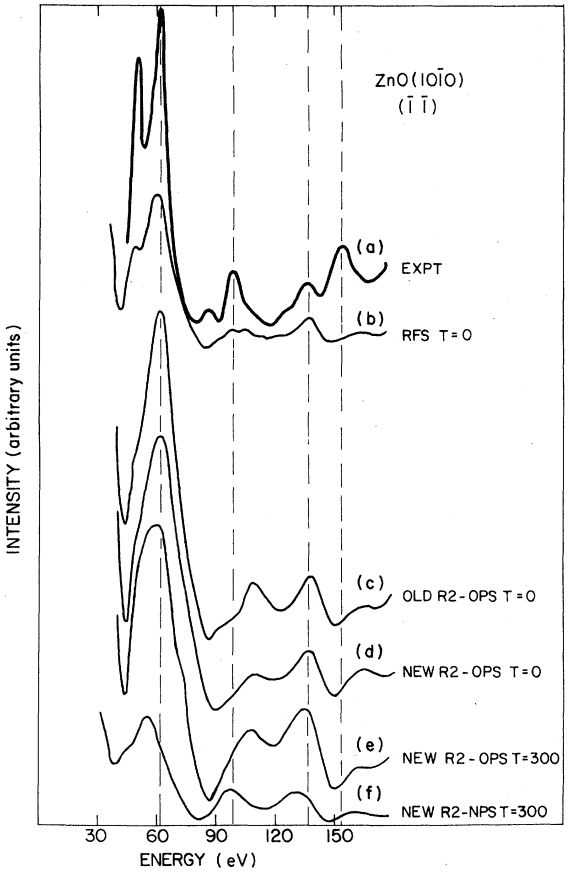

FIG. 10. Comparison of measured and calculated intensities of normally incident electrons diffracted into the (1$\bar{1}$) beam from ZnO(10$\bar{1}$0). Curve (a): measured intensities at $T = 300\,^{\circ}$K. Curve (b): RFS computation for a rigid lattice based on the OPS used by Duke *et al.* (Ref. 4) and the R2 reconstruction of the OS of Wyckoff (Ref. 12). Curve (c): the MI calculation utilizing the same model parameters as the RFS calculation shown in curve (b). Curve (d): rigid-lattice MI calculation based on the R2 reconstruction of the new (bulk) structure of Abrahams and Bernstein (Ref. 7). Curve (e): same as curve (d) but for $T = 300$ K. Curve (f): same as curve (e) but utilizing the NPS obtained from model 1, described in the text.

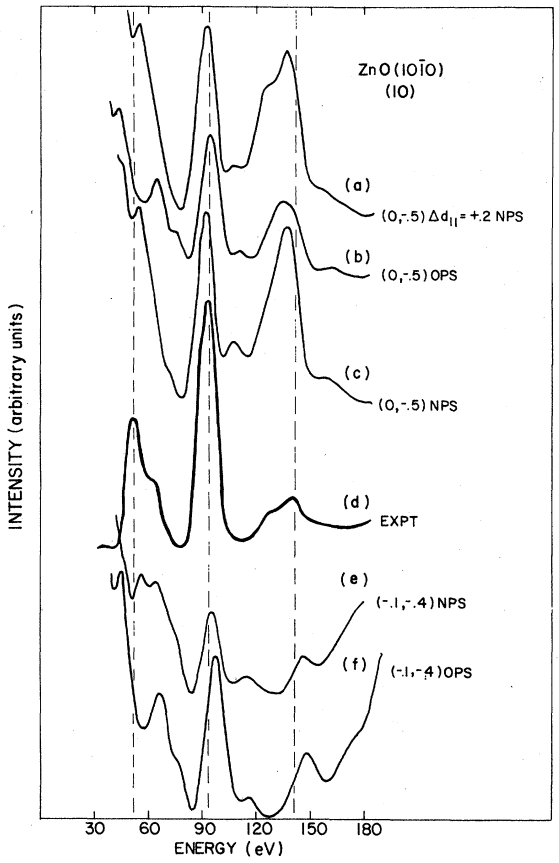

FIG. 11. Comparison of calculated and measured intensities of the (10) beam of normally incident electrons diffracted from ZnO(10$\bar{1}$0). Curve (a): calculated curve using the bulk geometry of Abrahams and Bernstein, (Ref. 7) the potential obtained from model 1 described in the text, and the first-layer distortion described by $\Delta d_{\perp}(\mathrm{O}) = 0$, $\Delta d_{\perp}(\mathrm{Zn}) = -0.5$ Å, $\Delta d_{\parallel}(\mathrm{Zn}) = 0.2$ Å. Curve (b): same as curve (a) but evaluated using the potential obtained from model 2 described in the text and $\Delta d_{\perp}(\mathrm{O}) = 0$, $\Delta d_{\perp}(\mathrm{Zn}) = -0.5$ Å, $\Delta d_{\parallel}(\mathrm{Zn}) = 0$. Curve (c): same as curve (b) but evaluated using the potential constructed via model 1 described in the text. Curve (d): measured intensities. Curve (e): same as curve (c) but with $\Delta d_{\perp}(0) = -0.1$ Å, $\Delta d_{\perp}(\mathrm{Zn}) = -0.4$ Å. Curve (f): same as curve (e) but evaluated using the potential obtained from model 2 described in the text.

study. Their consequence for our structure analyses described in Sec. III, however, is that we require only qualitative correspondence between the calculated and observed intensities in this energy range. For 60 eV $\lesssim E \lesssim$ 180 eV, the major features of the observed intensities are reproducible to within ±3–5 eV, although the detailed line shapes can change somewhat from one measurement to the next. Figure 6 provides a useful reference both for comparisons of measured and calculated ELEED intensities and for the assessment of the significance of variations in the calculated ELEED intensities associated with uncertainties in the model electron-solid force law.

The major conclusion emanating from our examination of the dependence of the calculated intensities on the choice of model electron-solid interaction is that the magnitude of alterations in the calculated ELEED intensities resulting either

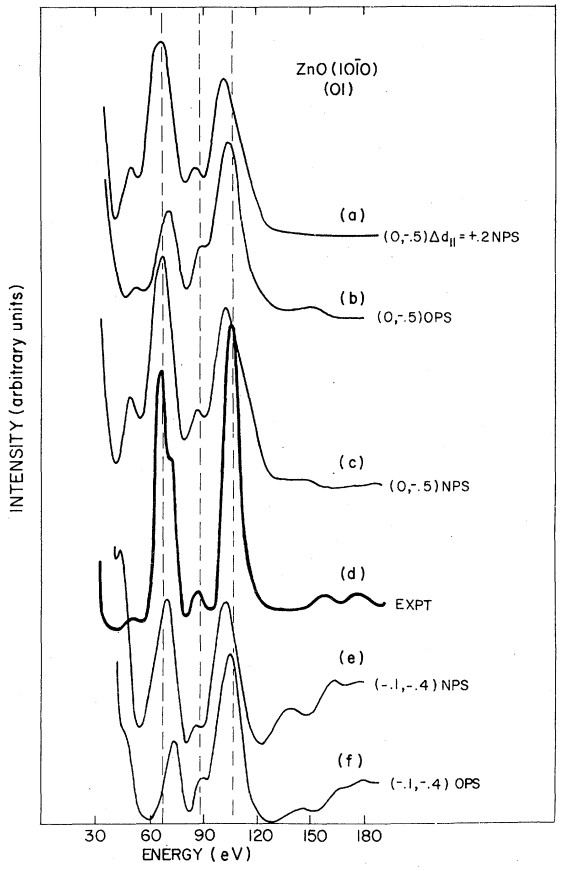

FIG. 12. Comparison of calculated and measured intensities of the (01) beam of normally incident electrons diffracted from ZnO(10$\bar{1}$0). Curve (a): calculated curve using the bulk geometry of Abrahams and Bernstein (Ref. 7), the potential obtained from model 1 described in the text, and the first-layer distortion described by $\Delta d_{\perp}$ (O) = 0, $\Delta d_{\perp}$ (Zn) = − 0.5 Å, $\Delta d_{\parallel}$ (Zn) = 0.2 Å. Curve (b): same as curve (a) but evaluated using the potential obtained from model 2 described in the text and $\Delta d_{\perp}$ (O) = 0, $\Delta d_{\perp}$ (Zn) = − 0.5 Å, $\Delta d_{\parallel}$ (Zn) = 0. Curve (c): same as curve (b) but evaluated using the potential constructed via model 1 described in the text. Curve (d): measured intensities. Curve (e): same as curve (c) but with $\Delta d_{\perp}$ (O) = − 0.1 Å, $\Delta d_{\perp}$ (Zn) = − 0.4 Å. Curve (f): same as curve (e) but evaluated using the potential obtained from model 2 described in the text.

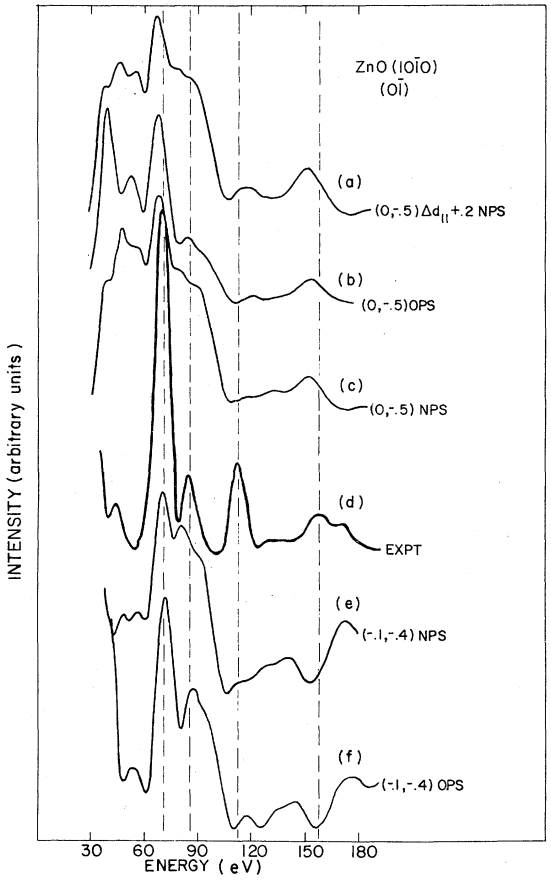

FIG. 13. Comparison of calculated and measured intensities of the (0$\bar{1}$) beam of normally incident electrons diffracted from ZnO(10$\bar{1}$0). Curve (a): calculated curve using the bulk geometry of Abrahams and Bernstein (Ref. 7), the potential obtained from model 1 described in the text, and the first-layer distortion described by $\Delta d_{\perp}$ (O) = 0, $\Delta d_{\perp}$ (Zn) = − 0.5 Å, $\Delta d_{\parallel}$ (Zn) = 0.2 Å. Curve (b): same as curve (a) but evaluated using the potential obtained from model 2 described in the text and $\Delta d_{\perp}$ (O) = 0, $\Delta d_{\perp}$ (Zn) = − 0.5 Å, $\Delta d_{\parallel}$ (Zn) = 0. Curve (c): same as curve (b) but evaluated using the potential constructed via model 1 described in the text. Curve (d): measured intensities. Curve (e): same as curve (c) but with $\Delta d_{\perp}$ (O) = − 0.1 Å, $\Delta d_{\perp}$ (Zn) = − 0.4 Å. Curve (f): same as curve (e) but evaluated using the potential obtained from model 2 described in the text.

from changes in the nonstructural parameters or from the use of the two different structures for bulk ZnO vary widely from one beam to another. Some beams, like the (01) beam shown in Fig. 7, are insensitive to any of these changes, including the choice of computational technique as already illustrated in Fig. 5. Others, like the (0$\bar{1}$) beam shown in Fig. 8, exhibit structurally significant changes in shape with changes in computational method (Fig. 5), temperature [panel (b), Fig. 8], and model potential [panels (c) and (d), Fig. 8]. In fact, for such beams the choice of bulk structure for ZnO is far less significant than that of the model potential or model of the atomic thermal vibrations. This type of knowledge is critical

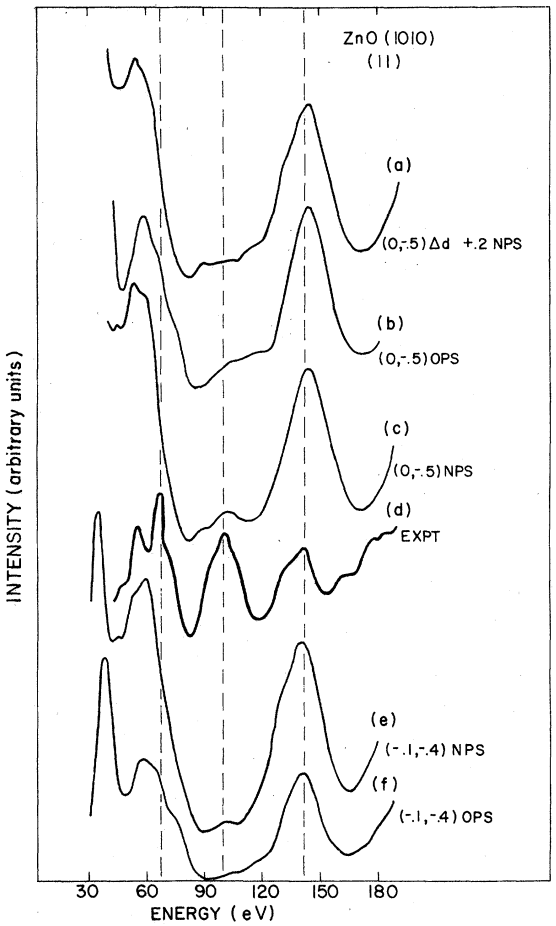

FIG. 14. Comparison of calculated and measured intensities of the (11) beam of normally incident electrons diffracted from ZnO(10$\bar{1}$0). Curve (a): calculated curve using the bulk geometry of Abrahams and Bernstein (Ref. 7), the potential obtained from model 1 described in the text, and the first-layer distortion described by $\Delta d_\perp(\mathrm{O}) = 0$, $\Delta d_\perp(\mathrm{Zn}) = -0.5$ Å, $\Delta d_\parallel(\mathrm{Zn}) = 0.2$ Å. Curve (b): same as curve (a) but evaluated using the potential obtained from model 2 described in the text and $\Delta d_\perp(\mathrm{O}) = 0$, $\Delta d_\perp(\mathrm{Zn}) = -0.5$ Å, $\Delta d_\parallel(\mathrm{Zn}) = 0$. Curve (c): same as curve (b) but evaluated using the potential constructed via model 1 described in the text. Curve (d): measured intensities. Curve (d): measured intensities. Curve (e): same as curve (c) but with $\Delta d_\perp(\mathrm{O}) = -0.1$ Å, $\Delta d_\perp(\mathrm{Zn}) = -0.4$ Å. Curve (f): same as curve (e) but evaluated using the potential obtained from model 2 described in the text.

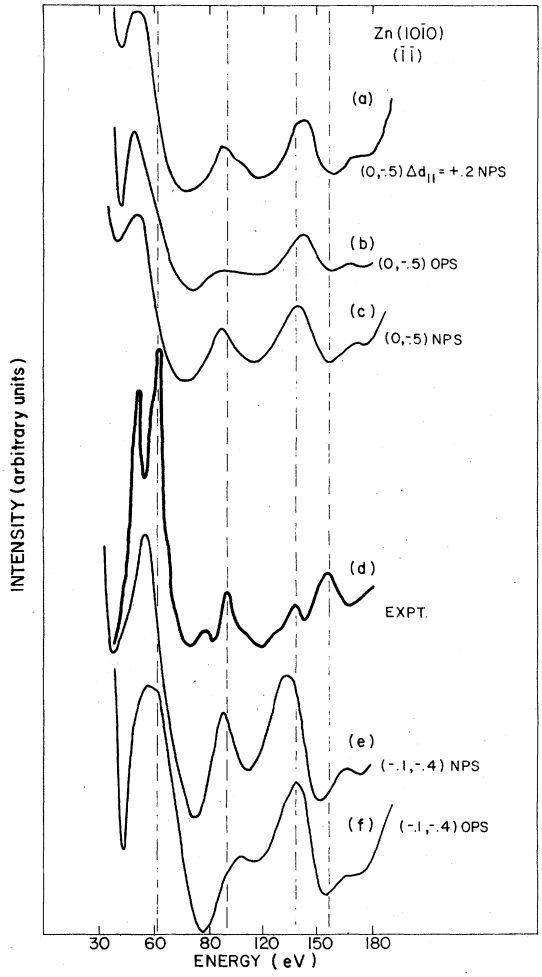

FIG. 15. Comparison of calculated and measured intensities of the ($\bar{1}\bar{1}$) beam of normally incident electrons diffracted from ZnO(10$\bar{1}$0). Curve (a): calculated curve using the bulk geometry of Abrahams and Bernstein (Ref. 7), the potential obtained from model 1 described in the text, and the first-layer distortion described by $\Delta d_\perp(\mathrm{O}) = 0$, $\Delta d_\perp(\mathrm{Zn}) = -0.5$ Å, $\Delta d_\parallel(\mathrm{Zn}) = 0.2$ Å. Curve (b): same as curve (a) but evaluated using the potential obtained from model 2 described in the text and $\Delta d_\perp(\mathrm{O}) = 0$, $\Delta d_\perp(\mathrm{Zn}) = -0.5$ Å, $\Delta d_\parallel(\mathrm{Zn}) = 0$. Curve (c): same as curve (b) but evaluated using the potential constructed via model 1 described in the text. Curve (d): measured intensities. Curve (e): same as curve (c) but with $\Delta d_\perp(\mathrm{O}) = -0.1$ Å, $\Delta d_\perp(\mathrm{Zn}) = -0.4$ Å. Curve (f): same as curve (e) but evaluated using the potential obtained from model 2 described in the text.

to achieving a reliable surface-structure analysis because the enhanced sensitivity of such beams to largely unknown nonstructural model parameters relative to the structural parameters renders their examination nearly useless for the purpose of determining atomic geometries.

Our calculations suggest, therefore, that, at least for ZnO(10$\bar{1}$0), the magnitude of changes in the intensities wrought by those in nonstructural parameters (especially the model muffin-tin potential) are more a property of the individual beam than of the energy of the incident electron, in contrast to results obtained earlier for metals

and overlayers thereon.[18,30-32] In particular, among those that we examined thoroughly, i.e., the (10) = ($\bar{1}$0), (01), (0$\bar{1}$), (11) = ($\bar{1}$1), and (1$\bar{1}$) = ($\bar{1}\bar{1}$) beams, the (0$\bar{1}$) beam proved extraordinarily sensitive to nonstructural parameters and hence a poor indicator of surface geometry; a conclusion which we illustrate in Fig. 9 for our previous best-fit structure, labeled by R2 in Duke *et al.*[4] Note in particular how major structural features in the intensities, e.g., the relative magnitudes of the three peaks at 75, 85, and 110 eV, are altered almost beyond recognition by utilizing model 1 rather than model 2 for the potential [panels (e) and (f), Fig. 9], whereas changing the bulk Zn-O spacing by 0.2 Å [panels (c) and (d), Fig. 9] create a smaller alteration in the calculated intensities than the choice of computational method [MI versus RFS, panels (b) and (c)]. Another important result illustrated in Fig. 9 is the obliteration of the peak at 110 eV by the onset of lattice vibrations. This is of particular significance for structure determinations on ZnO(10$\bar{1}$0) because no data on the temperature dependence of the ELEED intensities are available. Hence no model of the surface atomic vibrations can be firmly grounded in experimental observations. We conclude that although the (0$\bar{1}$) beam represents an extreme case of enhanced sensitivity of calculated ELEED intensities to nonstructural parameters, it provides an instructive example of the caution with which comparisons between a particular beam and experimental data must be regarded for a fixed model force law. In our original calculations[4] the (0$\bar{1}$) beam constituted one of the most pleasing examples of the improvement in the description of the measured intensities wrought by a reconstructed surface structure. The above analysis reveals graphically, however, the fortuitous nature of this conclusion which resulted, as it turned out, from special features of the computational method, the model potential, and the neglect of thermal vibrations.

While the (0$\bar{1}$) beam constitutes a useful example of the most severe limitations on the accuracy of an ELEED structure analysis of ZnO(10$\bar{1}$0), it is atypical. Most beams are considerably less sensitive to the values of the nonstructural parameters, as illustrated in Fig. 10 for the ($\bar{1}\bar{1}$) beam. The experimental uncertainties in the measured intensities for this beam were illustrated in Fig. 6. Comparison of Figs. 6 and 10 reveals that the experimental and "theoretical" uncertainties are quite comparable, which is usually the case in surface-structure determinations via ELEED intensity analyses. It is such uncertainties which limit the accuracy of ELEED structure analyses to $\Delta d \sim 0.1$ Å, although for a given electron-solid force law their precision can be higher.

III. STRUCTURE ANALYSIS

A. Procedure

Given the substantial effect of the model potential on the calculated ELEED intensities in certain beams, we performed again the entire structure analysis described by Duke *et al.*[2-4] using, however, the phase shifts associated with model 1 (as opposed to model 2) in Sec. II A and a vibrating lattice described by $\Theta_D = 385$ K, $T = 300$ K (as opposed to a rigid lattice). Initially, a complete range of single-layer reconstructions was examined corresponding to the Abrahams-Bernstein bulk ZnO geometry[7] modified by contractions of the oxygen- and zinc-layer spacings normal to the ZnO(10$\bar{1}$0) surface by $\Delta d_\perp(\mathrm{O}) \geq 0.2$ Å, $\Delta d_\perp(\mathrm{Zn}) < \Delta d_\perp(\mathrm{O})$, $\Delta d_\perp(\mathrm{Zn}) \geq -0.6$ Å. Comparisons with measured ELEED intensities were performed for the (01), (0$\bar{1}$), (10) = ($\bar{1}$0), (11) = ($\bar{1}$1), and (1$\bar{1}$) = ($\bar{1}\bar{1}$) diffracted beams associated with normally incident electrons. Analogous comparisons for nonnormally-incident electrons were not examined because of the poorer quality of the intensity data (higher background, large noise, inadequate reproducibility).

This initial search revealed two regions of structural parameters for which tolerable correspondence between the measured and calculated intensities was achieved: $\Delta d_\perp(\mathrm{O}) \cong 0$, $\Delta d_\perp(\mathrm{Zn}) \cong 0.5$ Å and $\Delta d_\perp(\mathrm{O}) \cong -0.1$ Å, $d_\perp(\mathrm{Zn}) \cong -0.4$ Å. These two regions of structural parameters were explored further by considering both translations of the Zn sublattice parallel to the surface along the y axis (i.e., $\Delta d_y \equiv \Delta d_\parallel \neq 0$; $\Delta d_x \equiv 0$ by symmetry of the spot pattern[2-4]), and second-layer distortions of both the oxygen and zinc sublattices by $|\Delta d_\perp| \leq 0.2$ Å. These refinements did not, in our judgment, make any improvement in the correspondence between the calculated and measured intensities lying outside the uncertainties described in Sec. II C.

In the following two subsections we present the most satisfactory comparisons between the calculated and observed intensities which emerged from these searches in the space of structural parameters for the fixed nonstructural parameters associated with model 1 as described in Sec. II A. We also show the calculated intensities resulting from these best-fit structural parameters (i.e., obtained using model 1) together with the nonstructural parameters of model 2 (Sec.

II A), so that the magnitude of the uncertainties associated with the choice of a particular model for the electron-solid force law are displayed explicitly.

B. Single-layer reconstructions

The calculated ELEED intensities for the two single-layer reconstructions which provided the best description of the observed normal-incidence diffracted intensities for ZnO($10\bar{1}0$) are compared with the measured intensities in Figs. 11–15. These figures illustrate the results for the (10) = ($\bar{1}0$), (01), ($0\bar{1}$), (11) = ($\bar{1}1$), and ($1\bar{1}$) = ($\bar{1}\bar{1}$) beams, respectively. The calculations for the two "best-fit" structures, i.e., $\Delta d_\perp(\mathrm{O}) = 0$, $\Delta d_\perp(\mathrm{Zn}) = -0.5$ Å and $\Delta d_\perp(\mathrm{O}) = -0.1$ Å, $\Delta d_\perp(\mathrm{Zn}) = -0.4$ Å are shown for the new phase shifts (NPS) obtained from model 1 and the original phase shifts (OPS) used by Duke *et al.*[2-4] and obtained from model 2. While the qualitative features of the calculated intensities are independent of the choice of phase shifts, the details of the (10), ($0\bar{1}$), (11), and ($1\bar{1}$) beams clearly depend on the model potential. Especially for the (10), ($0\bar{1}$), and ($1\bar{1}$) beams, any discrepancies between the calculated and measured intensities are comparable to those between the two sets of calculations themselves.

We also show in the uppermost panel of these figures the influence of a lateral translation of the uppermost Zn sublattice by 0.2 Å in such a fashion that it moves closer to its nearest-neighbor oxygen species in the surface layer as it sinks inward from the surface. This lateral motion corresponds to the R2 best-fit structure of Duke *et al.*[4] It is evident from Figs. 11–15 that little, if any, net improvement in the correspondence between the calculated and measured intensities is achieved by this translation. The improvement in the ($0\bar{1}$) beam is offset by diminutions in the quality of the descriptions of the (01) and (11) beams. We see that the predicted intensities are largely unchanged by this translation, however, an example of the general insensitivity of calculated ELEED intensities to reconstructions parallel to a surface relative to those normal to a surface. A complete grid of $-0.5 \leq \Delta d_\parallel(\mathrm{Zn}) \leq 0.5$ Å was examined during our analysis. Shifts of $\Delta d_\parallel$ by 0.1 Å create almost imperceptible changes in the calculated intensities, whereas those larger or of the opposite sign than the $\Delta d_\parallel = 0.2$ Å reconstruction, the consequences of which are shown in Figs. 11–15, decrease the correspondences between the calculated and measured intensities relative to those shown in the figures.

We conclude from a survey of single-layer reconstructions, epitomized by the results shown in Figs. 11–15, that the $\Delta d_\perp(\mathrm{O}) = 0$, $\Delta d_\perp(\mathrm{Zn}) = -0.5$ Å reconstruction affords the overall best description of the available (limited) data. Given the uncertainties in both the data (Fig. 5) and model force law, however, we cannot rule out contractions of the oxygen sublattice by as much as -0.1 ± 0.05 Å or that of the Zn sublattice by as little as -0.4 ± 0.05 Å, provided both occur together. Thus we assign $\Delta d_\perp(\mathrm{O}) = -0.05 \pm 0.1$ Å, $\Delta d_\parallel(\mathrm{O}) = 0 \pm 0.1$ Å, $\Delta d_\perp(\mathrm{Zn}) = -0.45 \pm 0.1$ Å, $\Delta d_\parallel(\mathrm{Zn}) = 0.1 \pm 0.2$ Å as the range of structural parameters consistent with the presently available normal-incidence ELEED intensity data.

The correspondence between the calculated and measured intensities, while adequate for most of the major features of the intensity profiles, is not as satisfactory for some of the smaller features as that obtained for certain metal surfaces.[30-32] Given the state of the art of surface preparation at the time when the intensities were measured (see, e.g., Fig. 6), this result is perhaps not surprising. Nevertheless, it is significant in this context that the single-layer reconstruction associated with the intensities shown in Figs. 11–15 were selected because for these structures the correspondence between the measured and calculated intensities is clearly best for all the beams, simultaneously. This result is illustrated in Figs. 16 and 17 for the ($0\bar{1}$) and (11) beams, respectively. It is this feature of the analysis which forms the primary basis for our conclusion that the failure of the computations to reproduce all the minor details in the measured intensity profiles lies in the combination of the quality of the data and the sensitivity of the calculations to the model force law, rather than to an incorrect structure.

C. Two-layer reconstructions

Given the recognition[6] that the reconstructions of Si and GaAs surfaces can penetrate as deeply as four atomic layers into the surface, it seemed appropriate to examine the possibility of such surface structures on ZnO($10\bar{1}0$) as well. In addition, multiple-layer reconstructions had been predicted for cubic ionic crystals by Bensen and Claxton a decade earlier.[33] Consequently, we performed a quite thorough search of second-layer reconstructions for top-layer atomic positions lying within the region $-0.1 \leq \Delta d_{\perp 1}(\mathrm{O}) \leq 0$ Å, $-0.6 \leq \Delta d_{\perp 1}(\mathrm{Zn}) \leq -0.3$ Å. The calculated ELEED intensities were examined for second-layer atomic positions throughout the parameter range $-0.2 \leq \Delta d_{\perp 2}(\mathrm{O})$

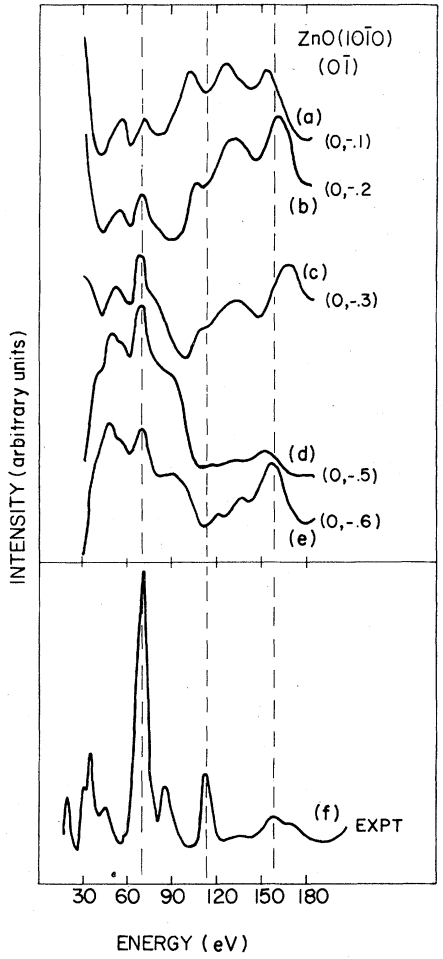

FIG. 16. Comparison of measured and calculated intensities of normally incident electrons diffracted into the (0$\bar{1}$) beam from ZnO(10$\bar{1}$0). Curve (a): calculated curve using the bulk geometry of Abrahams and Bernstein (Ref. 7), the potential obtained from model 1 described in the text, and the first-layer distortion described by $\Delta d_\perp(\mathrm{O}) = 0$, $\Delta d_\perp(\mathrm{Zn}) = -0.1$ Å. Curve (b): same as curve (a) but evaluated using $\Delta d_\perp(\mathrm{Zn}) = -0.2$ Å. Curve (c): same as curve (a) but evaluated using $\Delta d_\perp(\mathrm{Zn}) = -0.3$ Å. Curve (d): same as curve (a) but evaluated using $\Delta d_\perp(\mathrm{Zn}) = -0.5$ Å. Curve (e): same as curve (a) but evaluated using $\Delta d_\perp(\mathrm{Zn}) = -0.6$ Å. Curve (f): measured intensities at $T = 300\,^\circ$K.

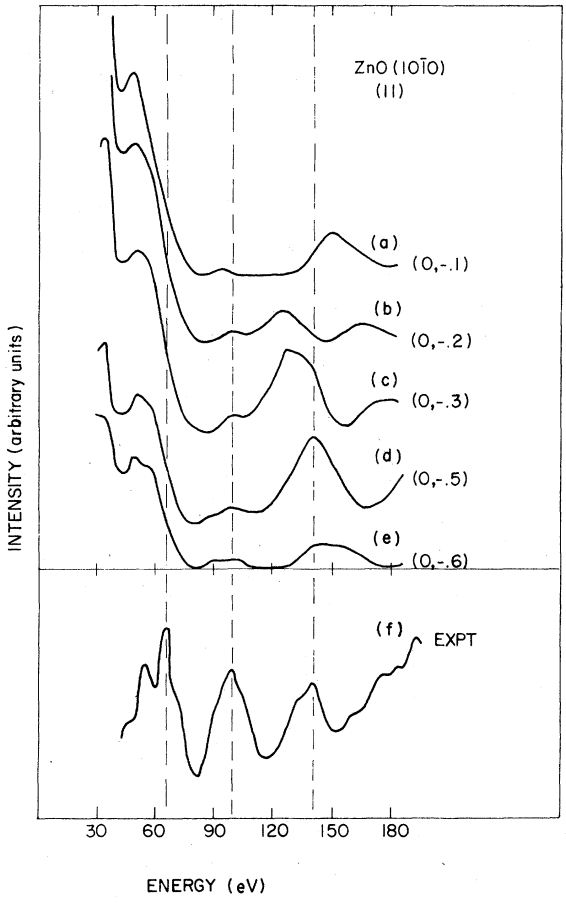

FIG. 17. Comparison of measured and calculated intensities of normally incident electrons diffracted into the (11) beam from ZnO(10$\bar{1}$0). Curve (a): calculated curve using the bulk geometry of Abrahams and Bernstein (Ref. 7), the potential obtained from model 1 described in the text, and the first-layer distortion described by $\Delta d_\perp(\mathrm{O}) = 0$, $\Delta d_\perp(\mathrm{Zn}) = -0.1$ Å. Curve (b): same as curve (a) but evaluated using $\Delta d_\perp(\mathrm{Zn}) = -0.2$ Å. Curve (c): same as curve (a) but evaluated using $\Delta d_\perp(\mathrm{Zn}) = -0.3$ Å. Curve (d): same as curve (a) but evaluated using $\Delta d_\perp(\mathrm{Zn}) = -0.5$ Å. Curve (e): same as curve (a) but evaluated using $\Delta d_\perp(\mathrm{Zn})$ 1$-$ 0.6 Å. Curve (f): measured intensities at $T = 300\,^\circ$K.

≤ 0.2 Å, $-0.2 \leq \Delta d_{\perp 2}(\mathrm{Zn}) \leq 0.2$ Å for a variety of upper-layer reconstructions.

The calculated intensities emanating from this search that exhibit the best correspondence with the measured ones are shown in Figs. 18–22 for the (10) = ($\bar{1}$0), (01), (0$\bar{1}$), (11) = ($\bar{1}$1) and, (1$\bar{1}$) = ($\bar{1}\bar{1}$) beams, respectively. Perhaps the best of these corresponds to $\Delta d_{\perp 1}(\mathrm{O}) = -0.1$ Å, $\Delta d_{\perp 2}(\mathrm{O}) = +0.1$ Å, $\Delta d_{\perp 1}(\mathrm{Zn}) = -0.5$ Å, and $\Delta d_{\perp 2}(\mathrm{Zn}) = 0$, shown in the upper panel of Figs. 18–22. We also show the $\Delta d_{\perp 1}(\mathrm{O}) = -0.1$ Å, $\Delta d_{\perp 1}(\mathrm{Zn}) = -0.4$ Å single-layer reconstruction in these figures for reference. While it can be argued that for certain beams [e.g., the (1$\bar{1}$) or (11) beams] the correspondence between the calculated and observed intensities

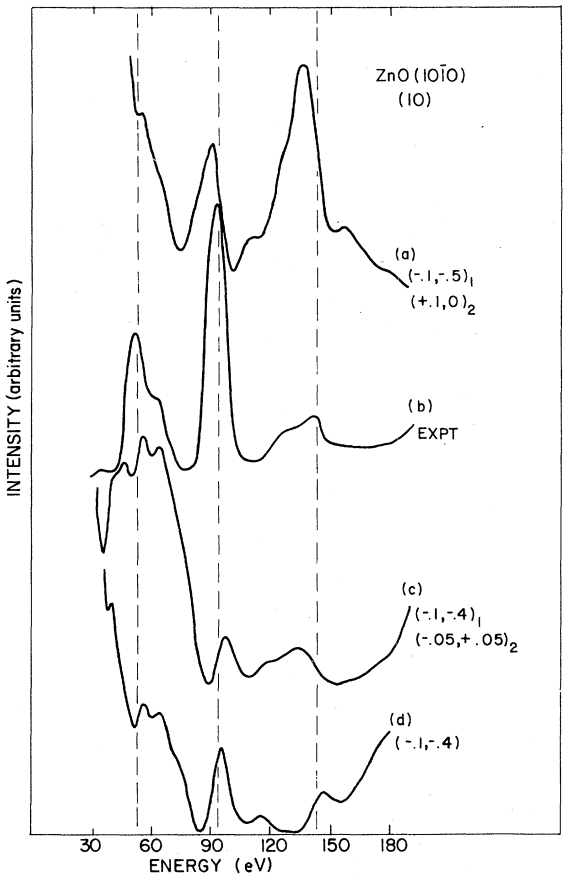

FIG. 18. Comparison of calculated and measured intensities of the (01) beam of normally incident electrons diffracted from ZnO(10$\bar{1}$0). Curve (a): calculated intensities evaluated using the potential obtained from model 1, described in the text, the Abrahams-Bernstein (Ref. 7) bulk geometry, a top-layer reconstruction of $\Delta d_{1\perp}(\mathrm{O}) = -0.1$ Å, $\Delta d_{1\perp}(\mathrm{Zn}) = -0.5$ Å and a second-layer reconstruction of $\Delta d_{2\perp}(\mathrm{O}) = +0.1$ Å, $\Delta d_{2\perp}(\mathrm{Zn}) = 0$. Curve (b): measured intensities. Curve (c): same as curve (a) but with the two-layer reconstruction described by $\Delta d_{1\perp}(\mathrm{O}) = -0.1$ Å, $\Delta d_{1\perp}(\mathrm{Zn})$ 1$-$ 0.4 Å, $\Delta d_{2\perp}(\mathrm{O}) = -0.05$ Å, $\Delta d_{2\perp}(\mathrm{Zn}) = +0.05$ Å. Curve (d) calculated intensites for the single-layer reconstruction most closely related to curves (a) and (c), i.e., $\Delta d_{1\perp}(\mathrm{O}) = -0.1$ Å, $\Delta d_{1\perp}(\mathrm{Zn}) = -0.4$ Å, $\Delta d_{2\perp}(\mathrm{O}) = \Delta d_{2\perp}(\mathrm{Zn}) = 0$.

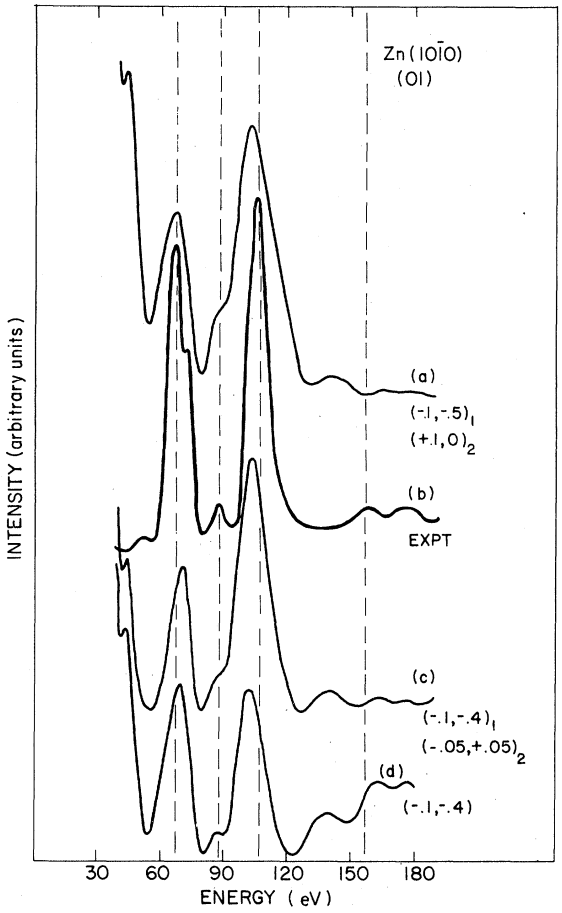

FIG. 19. Comparison of calculated intensities of the (01) beam of normally incident electrons diffracted from ZnO(10$\bar{1}$0). Curve (a): calculated intensities evaluated using the potential obtained from model 1, described in the text, the Abrahams-Bernstein (Ref. 7) bulk geometry, a top-layer reconstruction of $\Delta d_{1\perp}(\mathrm{O}) = -0.1$ Å, $\Delta d_{1\perp}(\mathrm{Zn}) = -0.5$ Å and a second-layer reconstruction $\Delta d_{2\perp}(\mathrm{O}) = +0.1$ Å, $\Delta d_{2\perp}(\mathrm{Zn}) = 0$. Curve (b): measured intensities. Curve (c): same as curve (a) but with the two-layer reconstruction described by $\Delta d_{1\perp}(\mathrm{O}) = -0.1$ Å, $\Delta d_{1\perp}(\mathrm{Zn}) = -0.4$ Å, $\Delta d_{2\perp}(\mathrm{O}) = -0.05$ Å, $\Delta d_{2\perp}(\mathrm{Zn}) = +0.05$ Å. Curve (d): calculated intensities for the single-layer reconstruction most closely related to curves (a) and (c), i.e., $\Delta d_{1\perp}(\mathrm{O}) = -0.1$ Å, $\Delta d_{1\perp}(\mathrm{Zn}) = -0.4$ Å, $\Delta d_{2\perp}(\mathrm{O}) = \Delta d_{2\perp}(\mathrm{Zn}) = 0$.

can be improved, that for other beams is simultaneously diminished. This is in contrast to single-layer reconstructions, which simultaneously improved the correspondence between theory and experiment for all beams. Moreover, none of the changes lie clearly outside the uncertainties, documented earlier, associated with the use of a particular model force law (model 1 in the case of Figs. 18–22).

We conclude, therefore, that in spite of our expectations to the contrary, the available normal-incidence ELEED intensity data do not require the occurrence of second-layer distortions for their interpretation.

IV. SYNOPSIS

In this paper we have reported a new surface-structure determination for ZnO(10$\bar{1}$0) via ELEED

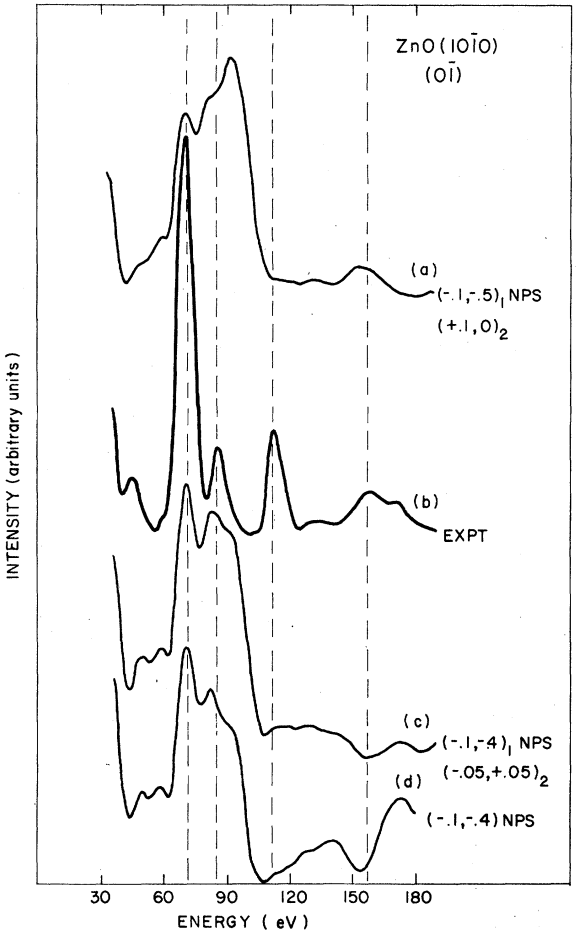

FIG. 20. Comparison of calculated and measured intensities of the (0$\bar{1}$) beam of normally incident electrons diffracted from ZnO(10$\bar{1}$0). Curve (a): calculated intensities evaluated using the potential obtained from model 1, described in the text, the Abrahams-Bernstein (Ref. 7) bulk geometry, a top-layer reconstruction of $\Delta d_{1\perp}(\mathrm{O}) = -0.1$ Å, $\Delta d_{1\perp}(\mathrm{Zn}) = -0.5$ Å and a second-layer reconstruction of $\Delta d_{2\perp}(\mathrm{O}) = +0.1$ Å, $\Delta d_{2\perp}(\mathrm{Zn}) = 0$. Curve (b): measured intensities. Curve (c): same as curve (a) but with the two-layer reconstruction described by $\Delta d_{1\perp}(\mathrm{O}) = -0.1$ Å, $\Delta d_{1\perp}(\mathrm{Zn}) = -0.4$ Å, $\Delta d_{2\perp}(\mathrm{O}) = -0.05$ Å, $\Delta d_{2\perp}(\mathrm{Zn}) = +0.05$ Å. Curve (d): calculated intensities for the single-layer reconstruction most closely related to curves (a) and (c), i.e., $\Delta d_{1\perp}(\mathrm{O}) = -0.1$ Å, $\Delta d_{1\perp}(\mathrm{Zn}) = -0.4$ Å, $\Delta d_{2\perp}(\mathrm{O}) = d_{2\perp}(\mathrm{Zn}) = 0$.

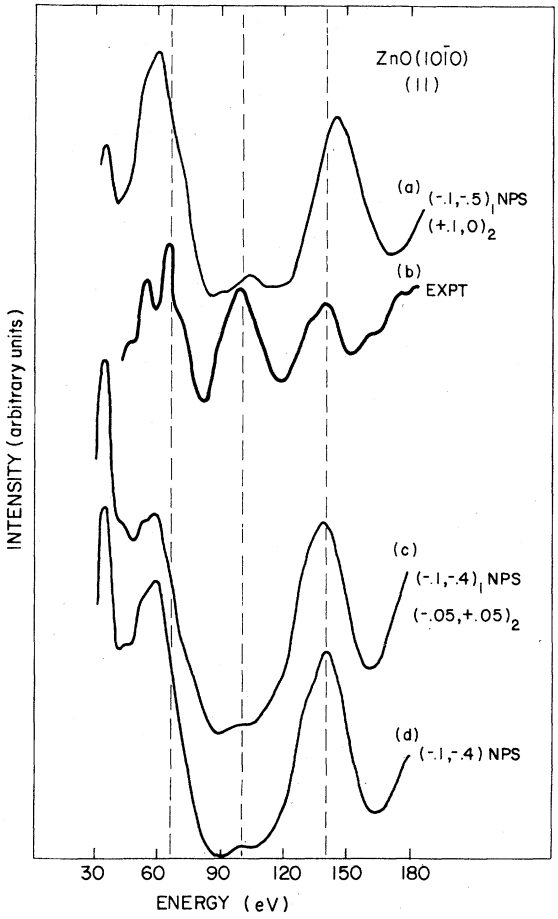

FIG. 21. Comparison of calculated and measured intensities of the (11) beam of normally incident electrons diffracted from ZnO(10$\bar{1}$0). Curve (a): calculated intensities evaluated using the potential obtained from model I, described in the text, the Abrahams-Bernstein (Ref. 7) bulk geometry, a top-layer reconstruction of $\Delta d_{1\perp}(\mathrm{O}) = -0.1$ Å, $\Delta d_{1\perp}(\mathrm{Zn}) = -0.5$ Å and a second-layer reconstruction of $\Delta d_{2\perp}(\mathrm{O}) = +0.1$ Å, $\Delta d_{2\perp}(\mathrm{Zn}) = 0$. Curve (b): measured intensities. Curve (c): same as curve (a) but with the two-layer reconstruction described by $\Delta d_{1\perp}(\mathrm{O}) = -0.1$ Å, $\Delta d_{1\perp}(\mathrm{Zn}) = -0.4$ Å, $\Delta d_{2\perp}(\mathrm{O}) = -0.5$ Å, $\Delta d_{2\perp}(\mathrm{Zn}) = +0.05$ Å. Curve (d): calculated intensities for the single-layer reconstruction most closely related to curves (a) and (c), i.e., $\Delta d_{1\perp}(\mathrm{O}) = -0.1$ Å, $\Delta d_{1\perp}(\mathrm{Zn}) = -0.4$ Å, $\Delta d_{2\perp}(\mathrm{O}) = \Delta d_{2\perp}(\mathrm{Zn}) = 0$.

intensity analysis, which represents an expansion of earlier work on this topic in five directions. First, a revised model of the electron–ion-core potential was introduced in which the prescription for determining the muffin-tin radii is taken to be the analog of that used in KKR band-structure calculations of ZnO.[24,25] Second, the sensitivity of the calculated ELEED intensities to the model potential was examined, and the resulting uncertainties in the comparisons between calculated and observed intensities were displayed explicitly in Figs. 9–15. Third, an extension of our MI computer program was reported which permits the examination of surface reconstructions which penetrate to an arbitrary depth from a semiconductor surface. Moreover, the results obtained using this "exact" MI method were compared with

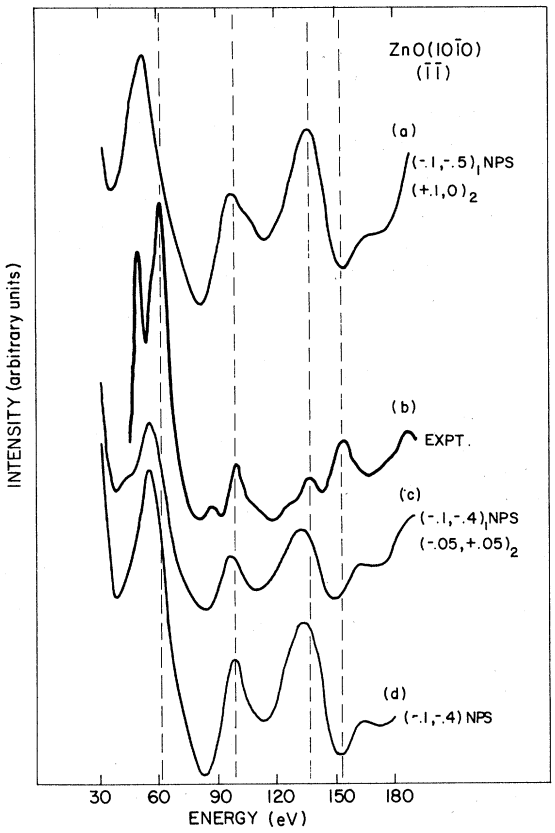

FIG. 22. Comparison of calculated and measured intensities of the ($\bar{1}\bar{1}$) beam of normally incident electrons diffraction from ZnO(10$\bar{1}$0). Curve (a): calculated intensities evaluated using the potential obtained from model 1, described in the text, the Abrahams-Bernstein (Ref. 7) bulk geometry, a top-layer reconstruction of $\Delta d_{1\perp}(\mathrm{O}) = -0.1$ Å, $\Delta d_{1\perp}(\mathrm{Zn}) = -0.5$ Å and a second-layer reconstruction of $\Delta d_{2\perp}(\mathrm{O}) = +0.1$ Å, $\Delta d_{2\perp}(\mathrm{Zn}) = 0$. Curve (b): measured intensities. Curve (c): same as curve (a) but with the two-layer reconstruction described by $\Delta d_{1\perp}(\mathrm{O}) = -0.1$ Å, $\Delta d_{1\perp}(\mathrm{Zn}) = 0.4$ Å, $\Delta d_{2\perp}(\mathrm{O}) = -0.05$ Å, $\Delta d_{2\perp}(\mathrm{Zn}) = +0.05$ Å. Curve (d): calculated intensities for the single-layer reconstruction most closely related to curves (a) and (c), i.e., $\Delta d_{1\perp}(\mathrm{O}) = 0.1$ Å, $\Delta d_{1\perp}(\mathrm{Zn}) = -0.4$ Å, $\Delta d_{2\perp}(\mathrm{O}) = \Delta d_{2\perp}(\mathrm{Zn}) = 0$.

those of the approximate RFS method, and the latter shown to be inadequate for the description of certain beams which are sensitive to details of the structure and potential (Fig. 5). Fourth, a revised bulk structure[7] for ZnO was employed *in lieu* of that given by Wyckoff,[12] which had been used earlier. Fifth, utilizing the new potential (model 1, Sec. II A) based on the revised ZnO structure,[7] we again performed a search of single- and double-layer reconstructions for ZnO(10$\bar{1}$0). The resulting ELEED intensities for the most probable structures are compared with normal-incidence intensity data in Figs. 11–22.

On the basis of our model calculations we conclude that the uppermost atomic layer of ZnO(10$\bar{1}$0) is reconstructed relative to the truncated bulk solid structure given by[7] the unit mesh $a_x = 3.25$ Å, $a_y = 5.21$ Å, and the atomic positions $d_{\perp,12} = 0.94$ Å, $d_{\perp,23} = 1.88$ Å, and $d_{y1}(\mathrm{Zn}) = 3.215$ Å relative to an oxygen species at the origin of the unit mesh. Specifically, we find that $d_{\perp,12}(\mathrm{O}) = 0.89 \pm 0.1$ Å, $d_{\perp,12}(\mathrm{Zn}) = 0.49 \pm 0.1$ Å and $d_{y1}(\mathrm{Zn}) = 3.315 \pm 0.2$ Å. On the basis of comparisons with the available normal-incidence ELEED intensity data we were unable to find any convincing evidence for second-layer distortions, however, although we suspect that they occur. Finally, the uncertainties in these surface geometries are large primarily because of the small amount of available ELEED intensity data, and in particular the lack of measurements of the temperature dependence of the ELEED intensities needed to establish a model of surface atomic vibrations. Further data is required before the structure can be refined further.

ACKNOWLEDGMENTS

This research was supported in part by ONR (N00014-75-C-0394), Army Research Office (DAAG29-77-G-0116), NSF (NSF-ENG75-18529), and the Mobil Oil Foundation.

[1]C. B. Duke and A. R. Lubinsky, Surf. Sci. 50, 605 (1975).
[2]A. R. Lubinsky, C. B. Duke, S. C. Chang, B. W. Lee, and P. Mark, J. Vac. Sci. Technol. 13, 189 (1976).
[3]C. B. Duke, A. R. Lubinsky, B. W. Lee, and P. Mark, J. Vac. Sci. Technol. 13, 761 (1976).
[4]C. B. Duke, A. R. Lubinsky, S. C. Chang, B. W. Lee, and P. Mark, Phys. Rev. B 15, 4865 (1977).
[5]C. B. Duke, J. Vac. Sci. Technol. 14, 870 (1977).
[6]C. B. Duke, Crit. Rev. Solid State Sci. (to be published).
[7]S. C. Abrahams and J. L. Bernstein, Acta Crystallogr. B 25, 1233 (1969).
[8]W. N. Unertl and J. M. Blakely, Surf. Sci. 69, 23 (1977).
[9]G. E. Laramore and C. B. Duke, Phys. Rev. B 5, 267 (1972).
[10]G. C. Kinniburgh, J. Phys. C 8, 2382 (1975).
[11]G. C. Kinniburgh and J. A. Walker, Surf. Sci. 63, 274 (1977).
[12]R. W. G. Wyckoff, *Crystal Structures* (Wiley, New York, 1963), Vol. I, pp. 111–112.

[13]C. H. Ehrhardt and K. Lark-Horovitz, Phys. Rev. 57, 603 (1940).
[14]R. A. Robie and J. L. Edwards, J. Appl. Phys. 37, 2659 (1966).
[15]J. L. Beeby, J. Phys. C 1, 82 (1968).
[16]C. B. Duke and G. E. Laramore, Phys. Rev. B 2, 4765 (1970); 25, 4783 (1970).
[17]C. B. Duke, D. L. Smith, and B. W. Holland, Phys. Rev. B 5, 3358 (1972).
[18]C. B. Duke, N. O. Lipari, and U. Landman, Phys. Rev. B 8, 2454 (1973).
[19]J. C. Slater, Phys. Rev. 81, 385 (1951); W. Kohn and L. J. Sham, Phys. Rev. 140, A1133 (1965).
[20]C. Kittel, *Introduction to Solid State Physics*, 2nd ed. (Wiley, New York, 1963), pp. 74–77.
[21]J. C. Slater, *Quantum Theory of Molecules and Solids* (McGraw-Hill, New York, 1965), Vol. II, p. 96.
[22]G. Cisneros-Stoianowski, Ph.D. thesis (Princeton University, April 1977) (unpublished).
[23]M. A. Bonn, Ph.D. thesis (Princeton University, June 1977) (unpublished).
[24]U. Rössler, Phys. Rev. 184, 733 (1969).
[25]U. Rössler and M. Lietz, Phys. Status Solidi 17, 597 (1966).
[26]J. L. Freeouf, Phys. Rev. B 7, 3810 (1973).
[27]L. Ley, A. Pollak, F. R. McFeely, S. P. Kowalczyk, and D. A. Shirley, Phys. Rev. B 9, 600 (1974).
[28]C. B. Duke and C. W. Tucker, Jr., Surf. Sci. 15, 231 (1969).
[29]S. C. Chang and P. Mark, Surf. Sci. 45, 721 (1974).
[30]C. B. Duke, Adv. Chem. Phys. 27, 1 (1974); *Dynamic Aspects of Surface Physics: Proceedings of the International School of Physics "Enrico Fermi" Course LVIII*, edited by F. O. Goodman (Editrice Compositori, Bologna, 1974), pp. 99–213.
[31]J. E. Demuth, P. M. Marcus, and D. W. Jepson, Phys. Rev. B 11, 1460 (1975).
[32]P. M. Marcus, J. E. Demuth, and D. W. Jepsen, Surf. Sci. 53, 501 (1975).
[33]G. C. Bensen and T. A. Claxton, J. Chem. Phys. 48, 1356 (1968).